substrate. This compares favorably with what would be expected as a result of the strong nonlinearity of the van der Waals potential, as can be seen by comparison with the simulation in Fig. 4C (*30*). The qualitative agreement is obvious.

An interesting question as to the spatial distribution of the holes arises from Fig. 4. At this stage of dewetting, the distribution appears to be quite random, similar to what is observed in the standard rupture scenario of polymer films (*6*). Does the correlation of the valley positions manifest itself noticeably in correlations of the hole positions, such that it is possible to distinguish the mechanism simply by analysis of their spatial distribution? The two-point correlation function of the hole positions does not reveal a significant difference between the spatial distribution of the holes in the gold film and those nucleated heterogeneously in a polymer film (*6*). However, by using the more elegant method of the so-called Minkowski measures, a clearer distinction becomes possible. Let us consider the centers of the holes in a film as an ensemble of points in the plane. On each point, let us put a circular disk, each with the same radius r, with its center on that point. Now let us consider the set defined as the set union of all disks. This is a complicated object whose geometrical properties depend on r. It is now useful to consider the morphological Minkowski measures of this object: its area, its boundary length, and its Euler characteristic (Fig. 5) (*31*). It turns out that these quantities, which are readily evaluated on a computer, are very sensitive to spatial correlations in the distribution of the initial ensemble of points.

In Fig. 5, we plotted these three quantities as a function of the disk radius, r. They are represented in a normalized form, such that the functional dependences for a purely random ensemble become simple. Aside from certain deviations in the boundary length (U^*), which can be attributed to the finiteness of the ensemble, the holes in the polymer film show good agreement with the predicted values for a purely random ensemble. In contrast, the data obtained with the gold film show substantial deviations. These data can be construed as confirming that the holes observed in the gold film are not generated by a random process such as heterogeneous nucleation, as the correlations in the hole positions are clearly visible by the strong deviation from the solid lines. They have formed instead from the valleys of the unstable undulation, which provides the observed correlation. However, the presence of the correlation in the spatial distribution of the hole positions demonstrates, in turn, that even though the appearance of the ensemble of holes may seem random at first glance, it inherited the specific correlations imposed by the spinodal process and may be identified by suitable methods such as the Minkowski measures.

References and Notes

1. G. Reiter, *Phys. Rev. Lett.* **68**, 75 (1992).
2. A. Sharma and A. T. Jameel, *J. Colloid Interface Sci.* **161**, 190 (1993).
3. M. Elbaum and S. G. Lipson, *Phys. Rev. Lett.* **72**, 3562 (1994).
4. G. Henn, D. G. Bucknall, M. Stamm, P. Vanhoorne, R. Jerome, *Macromolecules* **29**, 4305 (1996).
5. T. G. Stange, D. F. Evans, W. A. Hendrickson, *Langmuir* **13**, 4459 (1997).
6. K. Jacobs, S. Herminghaus, K. R. Mecke, *ibid.* **14**, 965 (1998).
7. R. Xie, A. Karim, J. F. Douglas, C. C. Han, R. A. Weiss, *Phys. Rev. Lett.* **81**, 1251 (1998).
8. We discuss only films with a thickness within the range of the dispersion forces, that is, not thicker than ~100 nm.
9. A. Vrij, *Discuss. Faraday Soc.* **42**, 23 (1966).
10. E. Ruckenstein and R. K. Jain, *Faraday Trans. II* **70**, 132 (1974).
11. F. Brochard-Wyart and J. Daillant, *Can. J. Phys.* **68**, 1084 (1990).
12. S. Dietrich, in *Phase Transitions and Critical Phenomena,* C. Domb and J. L. Lebowitz, Eds. (Academic Press, London, 1988), vol. 12, pp. 1–218.
13. M. Schick, in *Les Houches Session XLVIII, 1988: Liquids at Interfaces*, J. Charvolin *et al*., Eds. (Elsevier Science, Amsterdam, 1989), pp. 415–497.
14. J. W. Cahn, *J. Chem. Phys.* **42**, 93 (1965).
15. V. S. Mitlin, *J. Colloid Interface Sci.* **156**, 491 (1993).
16. J. Bischof, D. Scherer, S. Herminghaus, P. Leiderer, *Phys. Rev. Lett.* **77**, 1536 (1996).
17. M. Ibn-Elhaj, H. Möhwald, M. Z. Cherkaoui, R. Zniber, *Langmuir* **14**, 504 (1998).
18. R. Riegler and M. Engel, *Ber. Bunsenges. Phys. Chem.* **95**, 1424 (1991).
19. The influence of the dipolar polarizability of the subphase on long-range wetting forces has been shown in studies on the wetting of pentane on water [K. Ragil, J. Meunier, D. Broseta, J. Indekeu, D. Bonn, *Phys. Rev. Lett.* **77**, 1532 (1996)], among others.
20. Ripening of these structures was too slow to be observed on experimental time scales.
21. The possibility of imaging polar liquids has recently been demonstrated [A. Fery and S. Herminghaus, *Ultramicroscopy* **69**, 211 (1997)].
22. The system thus relaxes toward a film of finite thickness, that is, incomplete wetting. This justifies the well-established term "dewetting," even though the process does not leave a perfectly dry surface.
23. B. M. Ocko, A. Braslau, P. S. Pershan, J. Als-Nielsen, M. Deutsch, *Phys. Rev. Lett.* **57**, 94 (1986).
24. P.-G. DeGennes, *Langmuir* **6**, 1448 (1990).
25. M. J. Godbole, A. J. Pedraza, D. H. Lowndes, J. R. Thompson, *Mater. Res. Soc. Symp. Proc.* **235**, 583 (1992).
26. D. J. Srolovitz and M. G. Goldiner, *J. Met.* **3**, 31 (1995).
27. An intermediate layer of a few monolayers of chromium (thickness <2 nm) was deposited to improve the adhesion of the films.
28. T. Iida and R. I. L. Guthrie, *The Physical Properties of Liquid Metals* (Oxford Univ. Press, Oxford, 1987).
29. For simple monatomic liquids such as gold, the liquid is not expected to slip along the substrate. In the absence of slippage, the holes grow linear with time [F. Brochard, P. G. DeGennes, H. Hervert, C. Redon, *Langmuir* **10**, 1566 (1994)].
30. R. Khanna and A. Sharma, *J. Colloid Interface Sci.* **195**, 42 (1997).
31. K. R. Mecke, T. Buchert, H. Wagner, *Astron. Astrophys.* **288**, 697 (1994).

32. Stimulating discussions with G. Reiter, A. Sharma, and P. Leiderer are gratefully acknowledged.

29 June 1998; accepted 15 September 1998

Control of Chemical Reactions by Feedback-Optimized Phase-Shaped Femtosecond Laser Pulses

A. Assion, T. Baumert,* M. Bergt, T. Brixner, B. Kiefer, V. Seyfried, M. Strehle, G. Gerber

Tailored femtosecond laser pulses from a computer-controlled pulse shaper were used to optimize the branching ratios of different organometallic photodissociation reaction channels. The optimization procedure is based on the feedback from reaction product quantities in a learning evolutionary algorithm that iteratively improves the phase of the applied femtosecond laser pulse. In the case of $CpFe(CO)_2Cl$, it is shown that two different bond-cleaving reactions can be selected, resulting in chemically different products. At least in this case, the method works automatically and finds optimal solutions without previous knowledge of the molecular system and the experimental environment.

When lasers were invented they were considered the ideal tool for microscopic control of chemical reactions, that is, selective cleavage or formation of chemical bonds (*1*, *2*). By exactly tuning the monochromatic laser light according to the local mode frequency of a specific chemical bond, it was thought that enough energy could be deposited in this specific mode to cause selective bond breakage (*3*). In most experiments, however, selectivity is lost because of rapid intramolecular energy redistribution (*1*). Several control schemes have been proposed that make use of the coherent nature of laser radiation. Known as "coherent control," these schemes access

Physikalisches Institut, Universität Würzburg, Am Hubland, 97074 Würzburg, Germany.

*Present address: Deutsches Zentrum für Luft- und Raumfahrt, 82230 Wessling, Germany.

the broad range of quantum interference effects. Brumer and Shapiro (*4*), for example, showed theoretically that in a quantum mechanical system simultaneous one- and three-photon excitation can lead to constructive or destructive interference of different reaction pathways, depending on the relative phase of the light waves. Experimental realizations have been carried out on atomic and small molecular systems (*5*). A somewhat different control scheme makes use of the rapid progress in ultrashort laser pulse technology. For example, Tannor, Kosloff, and Rice (*6*) suggested a "pump-dump" technique, which has been realized experimentally by several groups (*7*).

Both types of control schemes are based on a limited number of optimization parameters: the phase difference between the two lasers and the time delay between the pump and dump laser pulses, respectively. In more complex systems these parameters may not be sufficient. Shi, Woody, and Rabitz (*8*) proposed that in order to reach a specific reaction channel, the electric field of the laser pulse should be specifically designed and fitted to the molecule, such that the amplitudes of the different interfering vibrational modes add up in a given bond some time after the photoabsorption, causing its breakage. To calculate the electric fields of these control schemes, "optimal control theory" has been used (*9*). In this approach, an "objective functional," consisting of the specific product yield in a chemical reaction, is maximized with respect to the electric field by solving Schrödinger's equation. This iterative optimum-seeking process has been theoretically applied to small model systems. For chemically relevant large molecules, however, this approach fails because molecular potential energy surfaces are not known accurately enough. Moreover, it has proved to be extremely difficult to generate the complex laser fields exactly as demanded by the theory.

Judson and Rabitz (*10*) introduced an idea for directly including the experimental output in the optimization procedure. A suitable algorithm forms an ultrashort laser pulse, uses the desired output as feedback in a learning algorithm, and iteratively improves the applied laser field, thus letting the system itself solve its Schrödinger equation in real-time without any approximations, under the constraints set by the laboratory conditions. Evolutionary algorithms (*10*, *11*) and simulated annealing algorithms (*12*) were suggested to serve this purpose. Some implementations have been demonstrated for automated femtosecond pulse compression (*13*, *14*) and optimized electronic population transfer in a dye molecule (*15*). In a recent article the field of laser control of chemical reactions has been reviewed (*16*).

Here we report an experimental realization of the automated optimization of coherent control of independent chemical reaction channels. We use a computer-controlled femtosecond laser pulse shaper together with an evolutionary algorithm and feedback from the femtosecond laser-driven photodissociation reaction output. Observing directly the product yields, it is possible to achieve an optimization without having to deal with the electronic population transfer within the parent molecule. Reaction pathway branching ratios of different organometallic molecules are either maximized or minimized automatically, without any knowledge of the specific molecular Hamiltonian.

The femtosecond laser system used in our experiments is capable of producing pulses with a duration of 80 fs and an energy of 1 mJ, at a center wavelength of 800 nm and a repetition rate of 1 kHz. The pulses are modified in a pulse shaper based on the design of Weiner *et al.* (*17*), which is set up as a zero dispersion compressor (*18*) with a liquid crystal spatial light modulator (SLM) in its Fourier plane. The SLM contains 128 rectangular pixels whose refractive indices can be changed separately by applying specific voltages. In this way different optical path lengths can be introduced to the spatially separated spectral components of the laser pulse, resulting in a shift of the relative phases. The emerging pulses are then focused into a high-vacuum chamber where they interact with a molecular beam of the educt molecules, leading to different multiphoton ionization and fragmentation processes. The ionic products are detected with a reflectron time-of-flight (TOF) mass spectrometer (*19*) from which the product yields can be fed directly into the controlling computer algorithm through boxcar averagers (Fig. 1).

We use an evolutionary algorithm (*20*) to optimize the spectral phase of the femtosecond laser pulses. The "genetic configuration" of a single individual corresponds to the SLM pixel voltage encodings. An "individual's fitness" is set equal to the measured branching ratio of the two competing reaction channels, that is, to the ratio of the respective ion signals. The "environmental adaptation" is found in the shaped laser pulse's capability of producing the desired experimental output. In the course of the evolutionary process, the reaction product in the numerator is favored at the cost of the reaction product in the denominator, because in each generation only the fittest individuals are selected for reproduction. A detailed description of our implementation of an evolutionary algorithm is given elsewhere (*13*). The algorithm automatically finds the best configuration for the SLM under the given laboratory conditions, no matter how complicated the molecular response may be. Laser and molecular beam density fluctuations, as well as different input pulse shapes, are automatically accounted for because experimental changes simply favor different pulse-shaper configurations. The algorithm works directly with the voltage encodings and not with any kind of expansion of the phase function. Therefore, there is no need to calibrate the SLM.

Organometallic molecules are widely used as photocatalysts in many organic reactions (*21*). Another application is found in microelectronics, where complete photodissociation of these compounds is essential for thin ultrapure metal film growth on surfaces (*22*). Microscopic control of their different fragmentation reactions could open up new applications. We have chosen to perform experiments on two sample substances: $Fe(CO)_5$ (iron pentacarbonyl, CAS [13463-40-6]) and $CpFe(CO)_2Cl$ (dicarbonylchloro(η^5-cyclopentadienyl)iron, CAS [12107-04-9]).

The experiments on the well-studied $Fe(CO)_5$ molecule are carried out primarily to test our method for self-learning coherent control. We have shown previously (*23*) that absorption of 800-nm femtosecond laser radiation

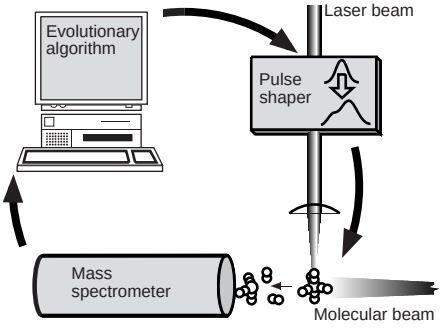

Fig. 1. Schematic experimental setup. Femtosecond laser pulses are modified in a computer-controlled pulse shaper. Ionic fragments from molecular photodissociation are recorded with a reflectron TOF mass spectrometer. This signal is used directly as feedback in the controlling evolutionary computer algorithm to optimize the branching ratios of photochemical reactions.

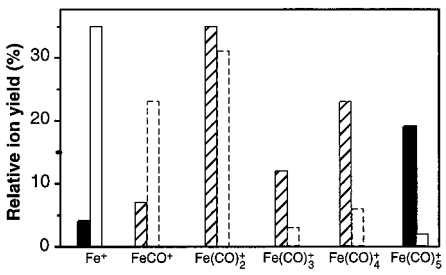

Fig. 2. Relative $Fe(CO)_5$ photodissociation product yields. The yields are derived from the relative peak heights of the mass spectra. The ratio of $Fe(CO)_5^+/Fe^+$ is maximized (solid blocks) as well as minimized (open blocks) by the optimization algorithm, yielding significantly different abundances of Fe^+ and $Fe(CO)_5^+$ in the two cases. The peak heights of all other masses [$FeCO^+$ up to $Fe(CO)_4^+$] have not been included in the optimization procedure.

induces different multiphoton ionization and fragmentation processes of this molecule, depending on the pulse duration. Direct ionization of the parent molecule occurs efficiently with ultrashort laser pulses of less than 100-fs duration. A more complex process consists of combined ionization and fragmentation in which the parent molecule loses not only an electron but also from one up to all five of its carbonyl ligands. Complete dissociation is predominantly initiated by long laser pulses of several picoseconds duration.

The branching ratio of two different exit channels [$Fe(CO)_5^+$ and Fe^+] was used as feedback signal in the automatic coherent control optimization scheme. Maximization is achieved within 30 generations of the evolutionary algorithm, yielding the product distribution of Fig. 2 (solid blocks). The result of this optimization is a very short (bandwidth-limited) laser pulse. If, on the other hand, we choose to minimize the $Fe(CO)_5^+/Fe^+$ ratio, that is, to maximize the inverse, an optimum is found almost immediately, after only very few generations (Fig. 2, open blocks). This optimization leads to a long laser pulse of picosecond duration. Several possible optimum pulse shapes (of picosecond pulse duration) are found by the algorithm that all yield the relative product distribution of Fig. 2 (open blocks). The individual mass peak heights depend on the experimental conditions, that is, the molecular beam density, the laser focus size, and so on, but the relative abundance of the undissociated $Fe(CO)_5^+$ in the minimization experiment is always significantly smaller than in the maximization experiment, and the relative abundance of the bare Fe^+ is simultaneously increased. The abundances of the other fragments were not included in the feedback signal. One can therefore not expect them to vanish or even to behave in any predictable way. Although some physical conclusions may still be drawn out of those proportions, our main objective was to control the $Fe(CO)_5^+/Fe^+$ ratio. The results are in complete agreement with previous experiments of pure pulse-length variation (*23*), indicating that the combination of our experimental methods with evolutionary optimization works well. The total photofragment yield in the minimization experiment is 10 times smaller than in the maximization experiment because the multiphoton-induced photodissociation is initiated by a long picosecond pulse with much lower laser intensity. However, the difference in fragment yield ratios $Fe(CO)_5^+/Fe^+$ by a factor of about 70 in the two experiments is not a mere intensity effect, because the $Fe(CO)_5^+/Fe^+$ ratio increases if the femtosecond laser beam intensity is lowered by attenuation at constant pulse duration (*23*).

In another experiment we examined the more complex molecule $CpFe(CO)_2Cl$, which incorporates different types of chemical metal-ligand bonds (Fe-CO, Fe-Cp, and Fe-Cl). One possible fragmentation channel of this molecule results in $CpFeCOCl^+$, by cleavage of one of the Fe-CO bonds. Another reaction channel leads to the $FeCl^+$ product where both carbonyl ligands as well as the Cp ligand have been removed. These two reaction pathways were the target of the coherent control optimization scheme. Other selections are also possible, but we wanted to explicitly demonstrate automated coherent control on products that are chemically different from each other and from the parent molecule. There are also some practical considerations in the selection of the target products, one of which is their absolute mass peak height.

The evolutionary algorithm was first used to maximize the $CpFeCOCl^+/FeCl^+$ branching ratio (Fig. 3, solid blocks). In contrast to the $Fe(CO)_5$ example, the corresponding laser pulse is not bandwidth-limited. Its interferometric autocorrelation (Fig. 4A) reveals a complex structure. In the $CpFeCOCl^+/FeCl^+$ minimization procedure, a significantly different product distribution is obtained (Fig. 3, open blocks). The branching ratio has dropped from 4.9 in the maximization experiment to 1.2 in the minimization experiment, and the resulting laser pulse shape has evidently changed (Fig. 4B). In an additional experiment we used an ultrashort (bandwidth-limited) laser pulse (Fig. 4C) and compared the $CpFeCOCl^+/FeCl^+$ ratio with those from the optimized laser pulses. The ratio in this case is only 2.4, proving that in the complex $CpFe(CO)_2Cl$ molecule (with different types of chemical bonds), simple bandwidth-limited laser pulses are not the best possible solution to the given problem. Arbitrarily shaped long laser pulses of picosecond duration do not yield an optimum ratio either.

Because our pulse shaper modulates only spectral phases and not amplitudes, the evolutionary algorithm produces optimized laser pulse shapes for a given pulse energy and for a given spectral intensity distribution. The fact that indeed the spectral optical phase and not

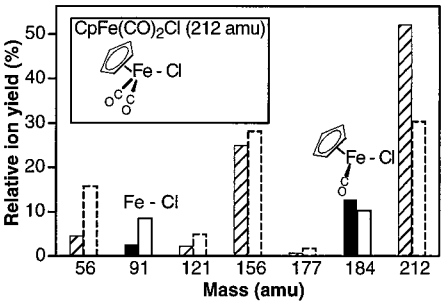

Fig. 3. Relative $CpFe(CO)_2Cl$ photodissociation product yields. Starting from the parent molecule, two different bond-breaking reactions are chosen that lead to chemically different final products. Their branching ratio, $CpFeCOCl^+/FeCl^+$, is maximized (solid blocks) as well as minimized (open blocks) by the optimization algorithm, yielding significantly different abundances of $CpFeCOCl^+$ and $FeCl^+$ in the two cases. The peak heights of the other fragments [Fe^+ (56), $CpFe^+$ (121), $CpFeCl^+$ (156), $CpFe(CO)_2^+$ (177)] and of the parent molecule $CpFe(CO)_2Cl^+$ (212) have not been included in the feedback signal.

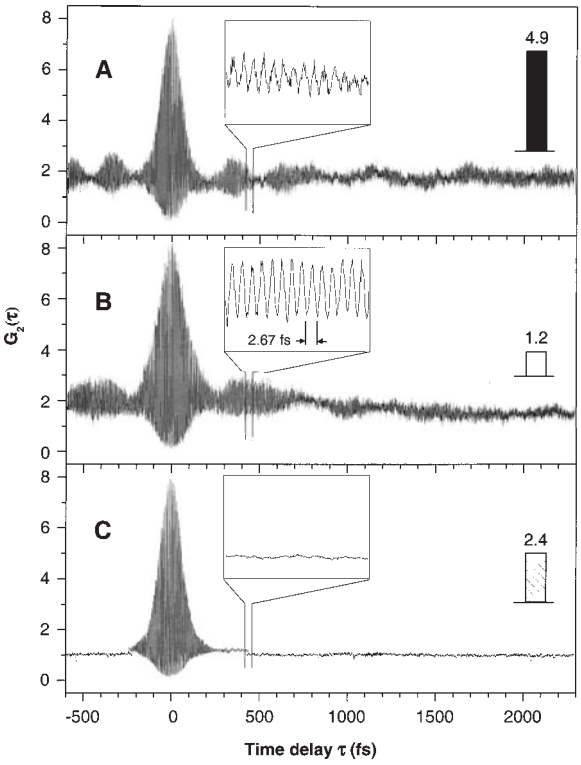

Fig. 4. Interferometric laser pulse autocorrelations. Second-order interferometric autocorrelation, $G_2(\tau) = \int [E(t - \tau) + E(t)]^4\, dt$, where $E(t)$ is the time-dependent real electric field, has been used to characterize the laser pulse shapes. Autocorrelations, which are always symmetric with respect to time, are shown for the $CpFeCOCl^+/FeCl^+$ maximization (**A**) and the minimization experiment (**B**). The product branching ratios are indicated by the figure inset blocks. The ratio obtained with a bandwidth-limited laser pulse (**C**) is inferior to the results obtained with the optimized pulses (A and B). Parts of the interferometric signals are shown in additional insets. One oscillation corresponds to the frequency of 800-nm laser radiation. The pulse-shape differences are clearly visible.

the pulse intensity is responsible for the optimization results can also be seen from the following argument. In the maximization as well as in the minimization experiment, the increased pulse duration leads to a reduced laser pulse intensity in the time domain as compared with the bandwidth-limited laser pulse. But in one case this reduction leads to a maximization, and in the other case it leads to a minimization, of the desired product branching ratio. It is therefore not possible to obtain the same or similar results by a trivial intensity reduction. Although it is not certain that the algorithm has found the global optimum, significant control between the two reaction channels was achieved, which cannot be obtained by a trivial adjustment of the laser pulse length or the laser pulse intensity.

The results demonstrate automated coherent control of photodissociation reactions with tailored femtosecond laser pulses from a computer-controlled pulse shaper. No information about the sample substance is needed in the optimization procedure, which always started with completely random genetic configurations. By directly optimizing different final product yields of bond-breaking reactions, we achieve a qualitative change from electronic population manipulation toward direct control of different reaction channels. The experiments reported here represent a step toward synthesizing chemical substances with higher efficiencies while at the same time reducing unwanted by-products.

References and Notes

1. W. S. Warren, H. Rabitz, M. Dahleh, *Science* **259**, 1581 (1993).
2. W. S. Warren, *ibid.* **262**, 1008 (1993); J. Manz and L. Wöste, Eds., *Femtosecond Chemistry* (VCH, Weinheim, Germany, 1995); P. Gaspard and I. Burghardt, Eds., *Chemical Reactions and Their Control on the Femtosecond Time Scale, XXth Solvay Conference on Chemistry* (Wiley, New York, 1997); R. J. Gordon and S. A. Rice, *Annu. Rev. Phys. Chem.* **48**, 601 (1997).
3. R. V. Ambartsumian and V. S. Letokhov, in *Chemical and Biochemical Applications of Lasers*, C. B. Moore, Ed. (Academic Press, New York, 1977), vol. 3, chapter 2; V. S. Letokhov, *Phys. Today* **30**, 23 (May 1977); N. Bloembergen and E. Yablonovitch, *ibid.* **31**, 23 (May 1978); A. H. Zewail, *ibid.* **33**, 27 (November 1980); J. Jortner, R. D. Levine, S. A. Rice, Eds., *Advances in Chemical Physics*, vol. 47, *Photoselective Chemistry* (Wiley, New York, 1981).
4. P. Brumer and M. Shapiro, *Chem. Phys. Lett.* **126**, 541 (1986); M. Shapiro, J. W. Hepburn, P. Brumer, *ibid.* **149**, 451 (1988); P. Brumer and M. Shapiro, *Chem. Phys.* **139**, 221 (1989).
5. C. Chen, Y.-Y. Yin, D. S. Elliott, *Phys. Rev. Lett.* **64**, 507 (1990); S. M. Park, S. P. Lu, R. J. Gordon, *J. Chem. Phys.* **94**, 8622 (1991).
6. D. J. Tannor and S. A. Rice, *J. Chem. Phys.* **83**, 5013 (1985); D. J. Tannor, R. Kosloff, S. A. Rice, *ibid.* **85**, 5805 (1986).
7. T. Baumert, M. Grosser, R. Thalweiser, G. Gerber, *Phys. Rev. Lett.* **67**, 3753 (1991); E. D. Potter, J. L. Herek, S. Pedersen, Q. Liu, A. H. Zewail, *Nature* **355**, 66 (1992); T. Baumert and G. Gerber, *Isr. J. Chem.* **34**, 103 (1994); J. L. Herek, A. Materny, A. H. Zewail, *Chem. Phys. Lett.* **228**, 15 (1994).
8. S. Shi, A. Woody, H. Rabitz, *J. Chem. Phys.* **88**, 6870 (1988).
9. A. P. Peirce, M. A. Dahleh, H. Rabitz, *Phys. Rev. A* **37**, 4950 (1988); R. Kosloff, S. A. Rice, P. Gaspard, S. Tersigni, D. J. Tannor, *Chem. Phys.* **139**, 201 (1989); W. Jakubetz, J. Manz, H.-J. Schreier, *Chem. Phys. Lett.* **165**, 100 (1990).
10. R. S. Judson and H. Rabitz, *Phys. Rev. Lett.* **68**, 1500 (1992).
11. B. Amstrup, G. J. Tóth, G. Szabó, A. Lörincz, *J. Phys. Chem.* **99**, 5206 (1995).
12. B. Amstrup, J. D. Doll, R. A. Sauerbrey, G. Szabó, A. Lörincz, *Phys. Rev. A* **48**, 3830 (1993).
13. T. Baumert, T. Brixner, V. Seyfried, M. Strehle, G. Gerber, *Appl. Phys. B* **65**, 779 (1997).
14. D. Yelin, D. Meshulach, Y. Silberberg, *Opt. Lett.* **22**, 1793 (1997).
15. C. J. Bardeen *et al.*, *Chem. Phys. Lett.* **280**, 151 (1997).
16. R. N. Zare, *Science* **279**, 1875 (1998).
17. A. M. Weiner, D. E. Leaird, J. S. Patel, J. R. Wullert II, *IEEE J. Quantum Electron.* **28**, 908 (1992).
18. O. E. Martínez, *ibid.* **24**, 2530 (1988).
19. B. A. Mamyrin, *Int. J. Mass Spectrom. Ion Processes* **131**, 1 (1994).
20. D. E. Goldberg, *Genetic Algorithms in Search, Optimization, and Machine Learning* (Addison-Wesley, Reading, UK, 1993); H.-P. Schwefel, *Evolution and Optimum Seeking* (Wiley, New York, 1995).
21. I. Wender and P. Pino, Eds., *Organic Synthesis via Metal Carbonyls* (Wiley, New York, 1977), vols. 1 and 2.
22. R. L. Jackson *et al.*, in *Laser Microfabrication*, D. J. Ehrlich and J. Y. Tsao, Eds. (Academic Press, New York, 1989), pp. 385–451.
23. L. Bañares, T. Baumert, M. Bergt, B. Kiefer, G. Gerber, *J. Chem. Phys.* **108**, 5799 (1998).

24. We gratefully acknowledge cooperation with the group of W. Malisch within the Sonderforschungsbereich 347 located at the University of Würzburg. Financial support of the Fonds der chemischen Industrie is also gratefully acknowledged.

8 June 1998; accepted 2 October 1998

The Effect of Alumina on the Electrical Conductivity of Silicate Perovskite

Yousheng Xu,* Catherine McCammon, Brent T. Poe

Measurements of the electrical conductivity of silicate perovskite at 25 gigapascals and 1400° to 1600°C show that the conductivity of (Mg,Fe)SiO_3 perovskite containing 2.89 weight percent Al_2O_3 is about 3.5 times greater than that of aluminum-free $(Mg_{0.915}Fe_{0.085})SiO_3$ perovskite. The conduction mechanism in perovskite between 1400° and 1600°C is most likely by polarons, because Mössbauer studies show that the aluminum-bearing perovskite has about 3.5 times the amount of Fe^{3+} as the aluminum-free sample. A conductivity-depth profile from 660 to 2900 kilometers based on aluminum-bearing perovskite is consistent with geophysical models.

The lower mantle consists predominantly of (Mg,Fe)SiO_3 perovskite coexisting with about 20% (Mg,Fe)O by volume. Aluminum is a minor element in the lower mantle, and it mainly goes into the perovskite phase (*1*). The partitioning of Fe and Mg between perovskite and magnesiowüstite is strongly coupled to Al_2O_3 concentration (*2*), and the proportion of Fe^{3+} in perovskite may increase greatly if perovskite contains a small amount of Al_2O_3 (*3*). If the conduction mechanism for perovskite is electron hopping from Fe^{2+} to Fe^{3+} (*4*), the electrical conductivity of perovskite should depend on the concentration of Fe^{3+} and is thus sensitive to substitution of Al_2O_3 into perovskite. Here, we evaluate this notion using in situ electrical conductivity measurements of perovskite at lower mantle conditions.

The starting materials for coexperiments were two polycrystalline pyroxene samples with similar Fe/(Fe + Mg) ratios: San Carlos $(Mg_{0.912}Fe_{0.088})SiO_3$ orthopyroxene containing 2.89% Al_2O_3 by weight and an Al-free synthetic orthopyroxene, $(Mg_{0.915}Fe_{0.085})SiO_3$. The samples were first transformed to perovskite at 25 GPa and 1600°C in a multianvil apparatus and then prepared as disks for in situ complex impedance spectroscopy in subsequent experiments at 25 GPa and 1400° to 1600°C (*5*).

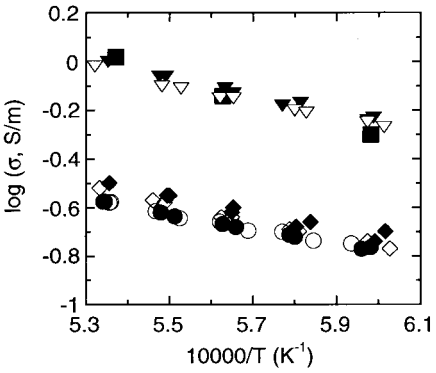

Fig. 1. Electrical conductivity of perovskite as a function of reciprocal temperature at 25 GPa. Squares and inverted triangles are for Al-bearing perovskite H826 and H858, respectively, and diamonds and circles are for Al-free perovskite H852 and H862, respectively. Closed symbols refer to the first heating and cooling cycle and open symbols refer to the second heating and cooling cycle.

Bayerisches Geoinstitut, Universität Bayreuth, D-95440 Bayreuth, Germany

*To whom correspondence should be addressed. E-mail: yousheng.xu@uni-bayreuth.de